Function and regulation of TRPP2 ion channel revealed by a gain-of-function mutant

Mahmud Arif Pavel[a], Caixia Lv[b], Courtney Ng[a], Lei Yang[c], Parul Kashyap[a], Clarissa Lam[a], Victoria Valentino[a], Helen Y. Fung[a], Thomas Campbell[a], Simon Geir Møller[a], David Zenisek[b], Nathalia G. Holtzman[d,e], and Yong Yu[a,1]

[a]Department of Biological Sciences, St. John's University, Queens, NY 11439; [b]Department of Cellular and Molecular Physiology, Yale University School of Medicine, New Haven, CT 06520; [c]Department of Physiology and Biophysics, Weill Cornell Medical College, New York, NY 10065; [d]Department of Biology, Queens College, City University of New York, Queens, NY 11367; and [e]The Graduate Center, City University of New York, New York, NY 10016

Edited by Lily Yeh Jan, University of California, San Francisco, CA, and approved March 14, 2016 (received for review August 27, 2015)

Mutations in polycystin-1 and transient receptor potential polycystin 2 (TRPP2) account for almost all clinically identified cases of autosomal dominant polycystic kidney disease (ADPKD), one of the most common human genetic diseases. TRPP2 functions as a cation channel in its homomeric complex and in the TRPP2/polycystin-1 receptor/ion channel complex. The activation mechanism of TRPP2 is unknown, which significantly limits the study of its function and regulation. Here, we generated a constitutively active gain-of-function (GOF) mutant of TRPP2 by applying a mutagenesis scan on the S4–S5 linker and the S5 transmembrane domain, and studied functional properties of the GOF TRPP2 channel. We found that extracellular divalent ions, including Ca^{2+}, inhibit the permeation of monovalent ions by directly blocking the TRPP2 channel pore. We also found that D643, a negatively charged amino acid in the pore, is crucial for channel permeability. By introducing single-point ADPKD pathogenic mutations into the GOF TRPP2, we showed that different mutations could have completely different effects on channel activity. The in vivo function of the GOF TRPP2 was investigated in zebrafish embryos. The results indicate that, compared with wild type (WT), GOF TRPP2 more efficiently rescued morphological abnormalities, including curly tail and cyst formation in the pronephric kidney, caused by down-regulation of endogenous TRPP2 expression. Thus, we established a GOF TRPP2 channel that can serve as a powerful tool for studying the function and regulation of TRPP2. The GOF channel may also have potential application for developing new therapeutic strategies for ADPKD.

autosomal dominant polycystic kidney disease | TRP channels | TRPP2 | polycystin | gain of function

Autosomal dominant polycystic kidney disease (ADPKD), one of the most common genetic diseases in humans, affects one in 400–1,000 individuals (1, 2). It is characterized by the formation of fluid-filled renal cysts that ultimately lead to kidney failure. ADPKD is caused by mutations in either the polycystin-1 or transient receptor potential polycystin 2 (TRPP2) protein (3). Polycystin-1, also known as PC1, a polycystic kidney disease (PKD) family member, is a large integral membrane protein with 11 transmembrane segments and a big extracellular N terminus (4). TRPP2, also known as polycystin-2 or PC2, is a member of the transient receptor potential (TRP) ion channel family, a large group of six-transmembrane cation channels that play crucial roles in sensory physiology (5, 6). Polycystin-1 and TRPP2 form a receptor/ion channel complex through the association of their C-terminal coiled-coil domains (7–10). Our previous work showed that this complex contains one polycystin-1 and three TRPP2 subunits (9, 10). How mutations in polycystin-1 or TRPP2 lead to ADPKD is unknown, but it is generally believed that the TRPP2/polycystin-1 complex functions as a sensor on primary cilia of renal epithelial cells to couple extracellular stimuli with intracellular Ca^{2+} signals (11–13). Presumably, disruption of this Ca^{2+} signaling leads to cyst formation in ADPKD. TRPP2 also forms a flow sensor with PKD1L1, another PKD protein, on the primary cilia of the embryonic nodal cells and plays a crucial role in establishing left/right asymmetry during early stages of development (14–17).

TRPP2 is a Ca^{2+}-permeable nonselective cation channel, and its channel function has been described both in the presence (12, 13, 18) and absence of polycystin-1 (19–21). TRPP2 is localized on multiple subcellular compartments, including the endoplasmic reticulum (ER) membrane, plasma membrane, and primary cilium, depending on the cell type or availability of binding partners (22). Correspondingly, TRPP2 appears to have distinct functions in each subcellular compartment (23, 24). For example, it functions as a calcium release channel on the ER membrane (21) and as a mechanosensitive channel in complex with polycystin-1 on the ciliary membrane (13). Due to the essential role of TRPP2 in ADPKD, understanding its channel function and regulation, and its role in renal physiology, are crucial. However, recording the TRPP2 current has been difficult, because TRPP2 is predominantly expressed in the ER instead of the plasma membrane (21, 25) and, more importantly, the activation mechanism of TRPP2 is still unknown. For this reason, almost all reported channel activity of TRPP2 is recorded at the single-channel level (19–21, 26–34), which has technical difficulties and limits the questions that can be addressed. The lack of a reliable system to record TRPP2 channel current easily has markedly delayed the study of this functionally important channel.

A gain-of-function (GOF) TRPP2 can bypass the activation mechanism. Thus, it will facilitate the study of function and regulation of TRPP2 and help unravel the downstream signaling pathways. In this study, we took a systematic mutagenesis approach to obtain a constitutively active GOF mutant of the TRPP2 channel. GOF mutations of other TRP channels identified

Significance

Mutations in transient receptor potential polycystin 2 (TRPP2) and polycystin-1 account for autosomal dominant polycystic kidney disease (ADPKD). TRPP2 is a cation channel and plays a crucial role in coupling extracellular stimuli to cellular responses in cells. The activation mechanism of TRPP2 is unknown, which significantly limits its study. Here, we report a gain-of-function (GOF) mutation that causes constitutive activity of TRPP2. This mutant was applied to investigation of the TRPP2 channel properties, the functional effects of ADPKD pathogenic TRPP2 mutations, and the in vivo function of the GOF TRPP2 in zebrafish embryos. From our results, we conclude that the GOF TRPP2 is a powerful tool for TRPP2 study, and has potential therapeutic applications in ADPKD treatment.

Author contributions: S.G.M., D.Z., N.G.H., and Y.Y. designed research; M.A.P., C. Lv, C.N., L.Y., P.K., C. Lam, V.V., H.Y.F., T.C., N.G.H., and Y.Y. performed research; M.A.P., N.G.H., and Y.Y. analyzed data; and M.A.P. and Y.Y. wrote the paper.

The authors declare no conflict of interest.

This article is a PNAS Direct Submission.

[1]To whom correspondence should be addressed. Email: yuy2@stjohns.edu.

This article contains supporting information online at www.pnas.org/lookup/suppl/doi:10.1073/pnas.1517066113/-/DCSupplemental.

in diseases or in random mutagenesis studies indicated a common gating feature among these channels: mutations in the linker between the fourth and fifth transmembrane segments (S4–S5 linker) and the first half of the fifth transmembrane segment (S5) can lead to constitutive channel activity (35) (Fig. S1). In a previous study, proline (Pro)-scanning mutagenesis conducted in this region successfully generated GOF mutants of the TRPML1 channel (36). We applied a similar strategy to TRPP2 and found F604P, a mutation in the S5 segment, causing constitutive opening of the TRPP2 channel when expressed in *Xenopus* oocytes. This GOF TRPP2 opens up an avenue for studies on TRPP2, as partially shown in this report. Our results not only provide new insights into the function and regulation of TRPP2 but also indicate a potential use for the GOF TRPP2 in new therapeutic strategies for ADPKD treatment.

Results

F604P Mutation Leads to GOF in the TRPP2 Channel. To obtain a GOF mutant of TRPP2, we carried out a systematic Pro mutagenesis screen in the last part of the S4–S5 linker and the first half of S5 (Fig. 1*A*). Mutated channels were expressed in *Xenopus* oocytes, and whole-oocyte currents were recorded in a divalent ion-free solution [100 mM NaCl, 2 mM Hepes-NaOH (pH 7.5)] using the two-electrode voltage clamp (TEVC) method. Among the 11 mutants, F604P gave significantly larger currents compared with WT and other mutant channels (Fig. 1 *B* and *C*). The permeability of the TRPP2_F604P channel to other monovalent ions was further measured in bath solutions containing 100 mM K^+, Li^+, Rb^+, or Cs^+. Compared with Na^+ solution, currents in the solutions with other ions have more positive reversal potential (Fig. 1*D*), indicating that the TRPP2_F604P mutant channel is more permeable to these cations ($P_{Na} : P_K : P_{Li} : P_{Rb} : P_{Cs} = 1:$

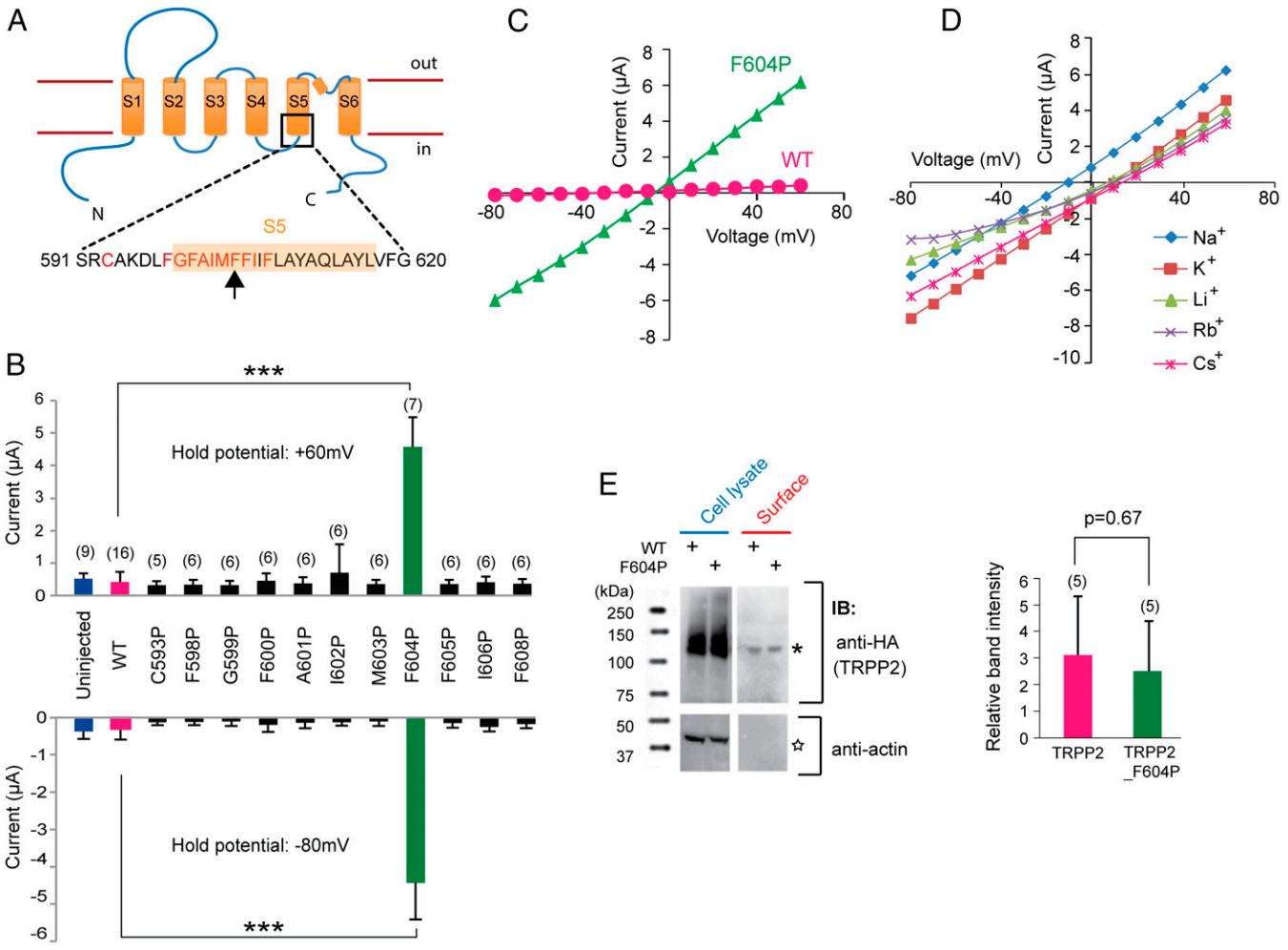

Fig. 1. Pro-scanning mutagenesis reveals a GOF mutant of TRPP2. (*A*) Putative transmembrane topology of TRPP2. The region that was selected for Pro-scanning mutagenesis, including the last part of the S4–S5 linker and the first half of S5, is marked with the black-lined box, and the corresponding amino acid sequence is indicated at the bottom. Amino acids that were substituted to Pro are in red. An arrow points to the amino acid F604. C, carboxyl terminus; N, amino terminus. (*B*) Bar graph showing inward and outward currents of TRPP2 mutants when expressed in *Xenopus* oocytes. Currents at −80 mV and +60 mV are shown. Recording was done in a standard divalent ion-free bath solution [100 mM NaCl, 2 mM Hepes-NaOH (pH 7.5)]. Numbers of tested oocytes are indicated in parentheses in this and the following figures. All data are shown as mean and SD, and significant difference was tested with Student's *t* test. ***$P < 0.001$. (*C*) Representative I-V curves of WT TRPP2 and F604P mutant. (*D*) Representative I-V curves of TRPP2_F604P when 100 mM of indicated ions was used in the divalent ion-free bath solution for recording. (*E*) TRPP2 and TRPP2_F604P have similar plasma membrane expression in *Xenopus* oocytes. (*Left*) Representative Western blot image. IB, immunoblot. Actin was blotted to show that only surface proteins were pulled down, and it also serves as a loading control. The asterisk and star indicate the positions of the expected protein bands of TRPP2 and actin, respectively. (*Right*) Bar graph shows relative intensity of Western blot bands of surface TRPP2 and TRPP_F604P proteins. Data come from five independent experiments, and no significant difference is found. Surface proteins were biotinylated and pulled down with streptavidin-coated beads.

2.2 : 1.9 : 2.2 : 2.4; $n = 6$). This result is consistent with previous reports, which showed that the TRPP2 channel is more permeable to K^+ and Rb^+ than Na^+ (20, 26, 37), although the calculated ratios vary in different studies.

Assuming the current we recorded is indeed conducted by TRPP2_F604P, three possible factors can result in the increased current of this mutant: higher expression of mutant channels on plasma membrane, an increase in channel open probability, or an increase in single-channel conductance. To clarify the effect of F604P further, we compared the plasma membrane expression of WT and F604P TRPP2 channels in *Xenopus* oocytes by purifying the biotinylated surface proteins. Results showed similar expression of WT and TRPP2_F604P in both oocyte lysate and plasma membranes (Fig. 1*E*), supporting the idea that the F604P mutation causes a GOF effect by increasing channel open probability or single-channel conductance.

Several lines of evidence further suggested that the current we recorded is indeed conducted by the TRPP2_F604P channel. First, the F604P mutation is necessary for GOF TRPP2 activity. Coexpression of WT TRPP2 RNA showed a dominant negative effect on the TRPP2_F604P current. When WT TRPP2 and TRPP2_F604P RNA were mixed in different ratios [WT:F604P = 100:0, 75:25, 50:50, 25:75, or 0:100 (%)] and injected together into oocytes, we found that the more WT RNA injected, the smaller were the currents recorded (Fig. 2*A*). Second, applying a mouse TRPP2 antibody (Ab), which recognizes the extracellular loop between the first and second transmembrane segments of TRPP2, partially inhibited the TRPP2_F604P current, whereas applying a mouse anti-GFP Ab did not (Fig. 2*B*). Third, the GOF function is F604P mutation-specific. We suspect that mutating F604 to Pro either breaks or kinks the S5 helix and locks the TRPP2 channel in an unregulated open state. Mutation of F604 to other hydrophobic amino acids that will keep the helix intact should not cause the same effect. Indeed, when F604 was mutated to either Ala (F604A) or Ile (F604I), the GOF effect was not observed (Fig. 2*C* and Fig. S2 *A* and *B*), although both mutants were expressed normally on oocyte plasma membrane (Fig. S2*C*). Fourth, ADPKD pathogenic mutations abolished TRPP2_F604P channel function. We tested the effect of two ADPKD-causing mutations on the current of TRPP2_F604P. D511V, a pathogenic missense mutation located at the bottom of the third transmembrane segment, has been shown previously to cause loss of TRPP2 channel activity (21, 38). When this mutation was introduced into TRPP2_F604P, we could no longer record any current (Fig. 2*D* and Fig. S2*D*). Similarly, the channel current was abolished when we introduced another pathogenic single-point deletion mutation located on S5, F605Δ (39) (Fig. 2*D* and Fig. S2*E*). F605Δ may cause dramatic local conformational changes that lead to closing of the channel gate. Finally, more direct evidence came from the results showing that mutations in the pore region of TRPP2_F604P caused ion selectivity changes (see Fig. 4 for data).

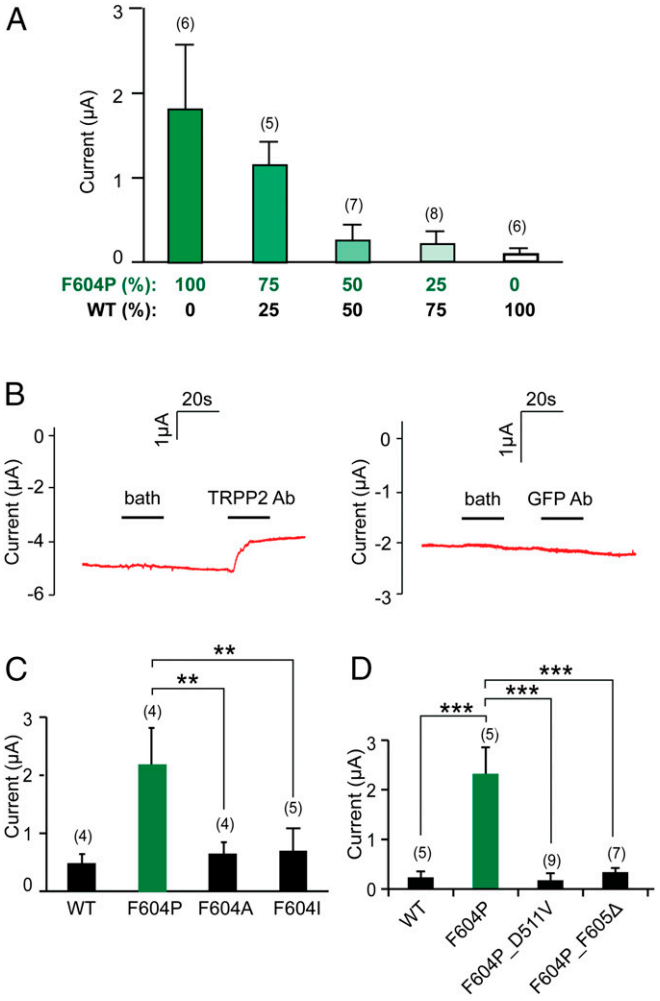

Fig. 2. Evidence showing that the current recorded from TRPP2_F604P RNA-injected oocytes is conducted by the TRPP2_F604P channel. (*A*) Bar graph showing the dominant negative effect of WT TRPP2 on TRPP2_F604P current when both RNAs were coinjected in *Xenopus* oocytes. The relative amounts of the two RNAs injected are indicated at the bottom. Average currents at +60 mV are shown in this graph, and in *C* and *D*. (*B*) Applying a mouse anti-TRPP2 Ab that recognizes the extracellular loop of TRPP2 partially inhibited TRPP2_F604P current (*Left*), whereas applying a mouse anti-GFP Ab did not (*Right*). Ooctyes were clamped at −60 mV. (*C*) Bar graph showing the lack of GOF effect produced by F604A and F604I. Representative I-V curves and proteins' surface expression are shown in Fig. S2. (*D*) Bar graph showing that two disease-causing mutations abolish TRPP2_F604P current. Representative I-V curves are shown in Fig. S2. Proteins' surface expression is shown, together with other disease-causing mutations, in Fig. 5C. $^{**}P < 0.01$; $^{***}P < 0.001$.

TRPP2_F604P Current Is Blocked by Common Cation Channel Blockers and Divalent Ions. The TRPP2_F604P mutant was further used to characterize the channel properties by examining the blocking effect of common channel blockers and divalent ions. Applying 0.5 mM Gd^{3+} or 5 mM amiloride greatly inhibited the GOF TRPP2 current (Fig. 3 *A* and *B*), consistent with a previous report on single-channel recording (19). Ruthenium Red (RuR), a ryanodine receptor inhibitor, was shown to block some TRP channels, such as TRPV1 (40), TRPV4 (41), and a heteromeric channel formed by TRPV4 and TRPP2 (42). Here, when we applied 100 μM RuR in bath solution, nearly complete inhibition of TRPP2_F604P current was observed (Fig. 3 *A* and *B*).

Along with being permeable through TRPP2, calcium regulates TRPP2 channel activity. Previous single-channel recordings showed that applying Ca^{2+} with a millimolar concentration on the extracellular side reduced the TRPP2 currents carried by monovalent cations (19, 20). However, this effect has not been well studied. A similar inhibitory effect by divalent ions was also found in the TRPP2/polycystin-1 complex channel (12) and in another TRPP family member, TRPP3 (43). We tested the effect of Ca^{2+} on the whole-oocyte current of TRPP2_F604P. When Ca^{2+} was added into the standard divalent ion-free bath solution, we noticed a significant reduction of the current, especially the inward current (Fig. 3 *C*–*E* and Fig. S3*A*). Conversely, when we added 5 mM EDTA in the extracellular solution to chelate the trace amounts of divalent ions, a slightly bigger current was recorded (Fig. 3 *C* and *D*). Both results indicate that extracellular Ca^{2+} blocks the conductance of monovalent ions.

The inhibitory effect of Ca^{2+} is strongly voltage-dependent, and an outwardly rectifying current was recorded in the presence

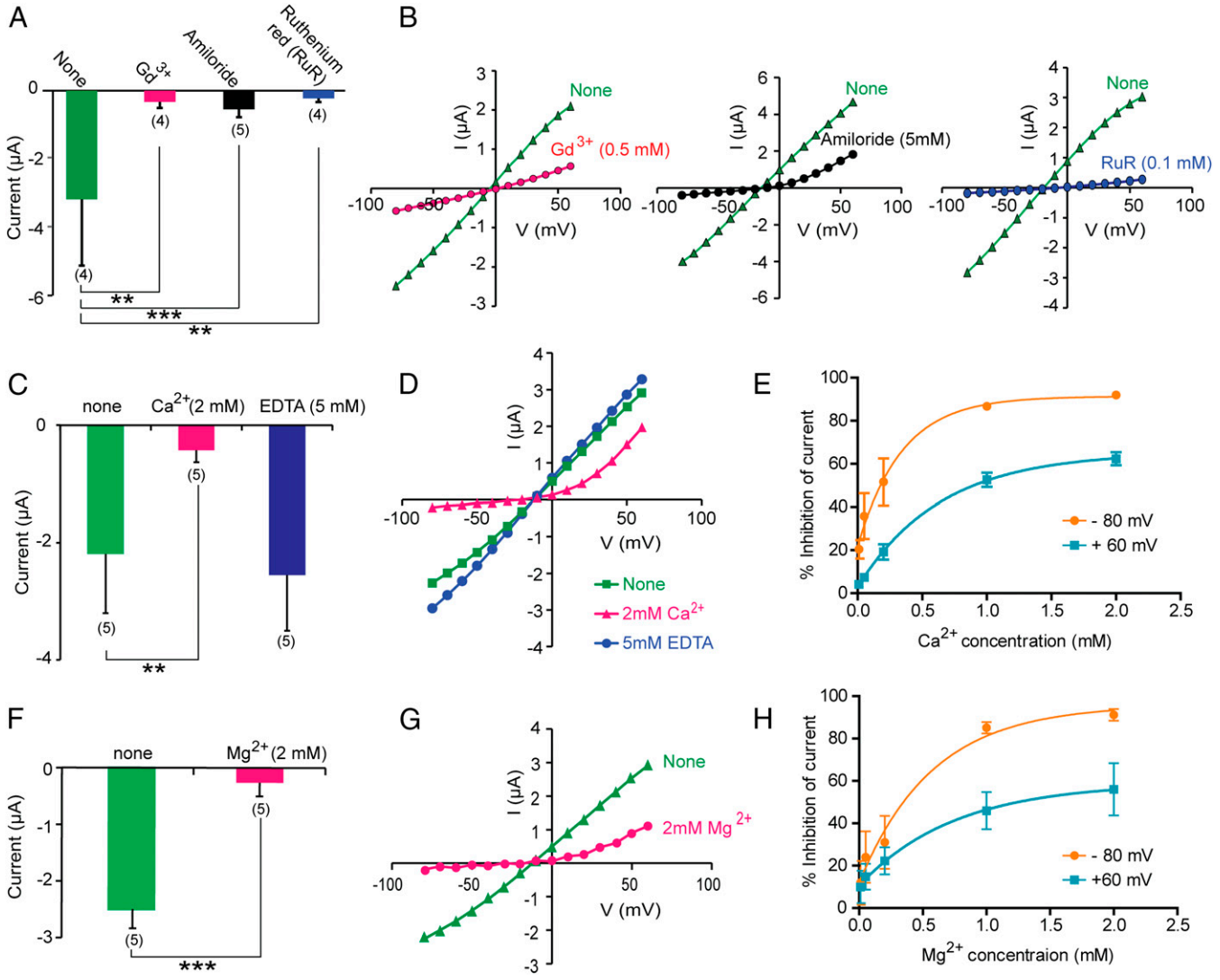

Fig. 3. TRPP2_F604P current is inhibited by common cation channel blockers and divalent ions. (*A*) Bar graph showing that the TRPP2_F604P current was inhibited by adding Gd^{3+} (0.5 mM), amiloride (5 mM), or RuR (0.1 mM) into standard divalent ion-free bath solution. Average currents at −80 mV are shown. (*B*) Corresponding representative I-V curves for the data in *A*. (*C* and *F*) Bar graphs show the inhibition of TRPP2_F604P inward current by extracellular 2 mM Ca^{2+} (*C*) or 2 mM Mg^{2+} (*F*), and the effect of 5 mM EDTA (*C*). (*D* and *G*) Representative I-V curves of TRPP2_F604P in divalent ion-free bath solution (labeled as "None") and solutions with 2 mM Ca^{2+} (*D*), 5 mM EDTA (*D*), or 2 mM Mg^{2+} (*G*) added are shown. (*E* and *H*) Concentration-dependent inhibition of inward (at −80 mV, orange traces) and outward (at +60 mV, blue traces) currents of the TRPP2_F604P by extracellular Ca^{2+} (*E*) and Mg^{2+} (*H*). Best-fit exponential curves are shown ($n = 5$ in both cases). Representative I-V curves under different concentration of Ca^{2+} are shown in Fig. S3*A*. $^{**}P < 0.01$; $^{***}P < 0.001$.

of extracellular Ca^{2+} (Fig. 3*D*), indicating a possible open-channel blocking mechanism. This current can be further blocked by 100 μM RuR (Fig. S3*B*). It is also possible that the remaining outward current is actually caused by the influx of Cl^- ions through endogenously expressed Ca^{2+}-activated chloride channels (44–46). To rule out this possibility, we replaced Cl^- in bath solution with gluconate$^-$, which is not permeable to chloride channels, and found no change in the outward current (Fig. S3 *C* and *D*). This result indicates that the outward current is indeed carried by cation (mainly K^+) efflux through the TRPP2_F604P channel. In a dose–response experiment, the inhibition of inward current reaches saturation when ∼1 mM Ca^{2+} is present extracellularly (Fig. 3*E* and Fig. S3*A*).

The effects of two other divalent ions, Mg^{2+} and Ba^{2+}, were tested. Mg^{2+} has a similar inhibition on the TRPP2_F604P current as Ca^{2+} (Fig. 3 *F*–*H*). However, Ba^{2+} caused more inhibition of both inward and outward currents than Ca^{2+} and Mg^{2+} (Fig. S3*E*). Divalent ions may inhibit the flow of monovalent ions by directly binding to negatively charged amino acids located in or close to the channel pore. If divalent ions inhibit TRPP2_F604P channel through a similar mechanism, then the greater inhibitory effect of Ba^{2+} indicates a strong affinity of Ba^{2+} to the binding site. However, it is also possible that Ba^{2+} has a different inhibition mechanism from Ca^{2+} and Mg^{2+}, because it also greatly inhibited the outward current.

Because Ca^{2+} binds less strongly to protonated carboxylic groups than to unprotonated carboxylic groups, low pH should weaken the binding of Ca^{2+} and reduce its blocking effect. In the cyclic nucleotide-gated (CNG) channel, lower pH has been shown to reduce Ca^{2+} inhibition (47). The effect of pH on the Ca^{2+} blocking of the TRPP2_F604P channel was tested, and results showed that both low (4.0) and high (9.0) pH have no significant effect on Ca^{2+} blocking, although they slightly decrease the outward current (Fig. S4*A*). The lack of effect of pH on Ca^{2+} blocking indicates either the binding site of Ca^{2+} is not accessible to H^+ or binding of H^+ itself also blocks the channel. Indeed, low pH

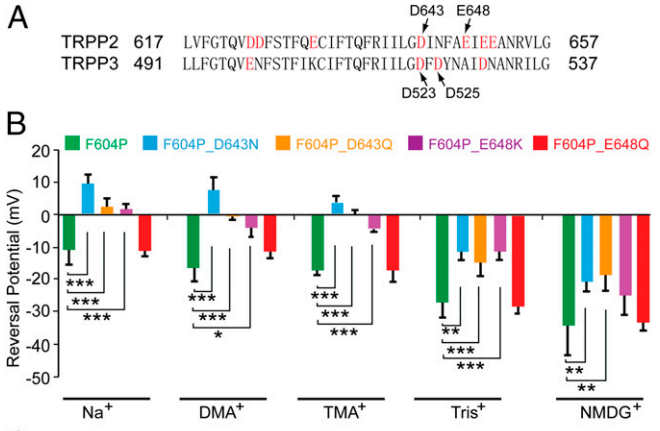

C

	P_{Na}/P_{NMDG}	P_{DMA}/P_{NMDG}	P_{TMA}/P_{NMDG}	P_{Tris}/P_{NMDG}
F604P	2.5	2.0	1.9	1.3
F604P_D643N	3.3	3.0	2.6	1.4
F604P_D643Q	2.3	2.0	2.1	1.2
F604P_E648K	2.8	2.3	2.2	1.7
F604P_E648Q	2.4	2.4	1.9	1.2

Fig. 4. D643 is critical for the ion selectivity of the TRPP2 channel. (*A*) Sequence alignment of the putative pore regions of human TRPP2 and TRPP3. Arrows indicate the two amino acids that are crucial for ion selectivity of the TRPP3/PKD1L3 channel (*Bottom*) and the two amino acids of TRPP2 that were mutated in this study (*Top*). (*B*) Bar graph showing the reversal potentials of currents recorded from TRPP2_F604P (green bars), F604P_D643N (blue bars), F604P_D643Q (orange bars), F604P_E648K (purple bars), and F604P_E648Q (red bars) in bath solutions containing 100 mM Na^+, DMA^+, TMA^+, $Tris^+$, or $NMDG^+$. $*P < 0.05$; $**P < 0.01$; $***P < 0.001$. (*C*) Relative permeability ratios of indicated ions to $NMDG^+$ in listed TRPP2 mutants. We chose $NMDG^+$ as the reference ion because its permeability has the smallest change among all ions when different mutants were tested. However, it should be noted that because the $NMDG^+$ permeability itself was increased in three of the four mutants, the permeability changes of other ions caused by these mutations are underestimated if one just compares the numbers in the table. More detailed results on the changes of both reversal potential and relative permeability ratios are listed in Table S1.

(pH 4) also inhibits the TRPP2_F604P current in the absence of Ca^{2+} (Fig. S4*B*). Low pH has been shown to inhibit TRPP3 activity in a previous study (48).

D643 Is Critical for Ion Selectivity of TRPP2. Next, the key amino acids in the channel pore for TRPP2 ion selectivity were explored. Negatively charged amino acids D523 and D525 play a crucial role in the cation selectivity of TRPP3 channel (49, 50). In TRPP2, D643 is aligned to D523 of TRPP3 (Fig. 4*A*), whereas another negatively charged amino acid, E648, is five amino acids downstream in the sequence (Fig. 4*A*). We hypothesized that these two amino acids may stay inside or close enough to the selectivity filter, and mutating them will change the ion selectivity of GOF TRPP2. To test this hypothesis, we mutated D643 to either Asn (N) or Gln (Q), and E648 to either Lys (K) or Q in TRPP2_F604P and measured the ion selectivity change caused by these mutations.

The reversal potential of TRPP2_F604P channel current in bath solution containing 100 mM Na^+ [molecular weight (MW) = 23] is -10.9 ± 4.6 mV (Fig. 4*B*, first green bar). When external Na^+ is replaced with bigger ions, including dimethylamine$^+$ (DMA^+; MW = 45.1), trimethylamine$^+$ (TMA^+; MW = 59.1), $Tris^+$ (MW = 121.1), or *N*-methyl-D-glucamine ($NMDG^+$; MW = 195.2), the reversal potentials shifted to -16.5 ± 4.1 mV, -17.2 ± 1.5 mV, -27.1 ± 4.7 mV, and -34.3 ± 9.1 mV, respectively (Fig. 4*B*, green bars), affirming the hypothesis that the bigger the size of the ions, the less permeable they are (Fig. 4*C*, permeability ratios of other ions to $NMDG^+$ in the row of F604P). $NMDG^+$ is still conducted by GOF TRPP2, although it is much less permeable than Na^+, indicating the relatively large size of the TRPP2 channel pore, which is consistent with previous reports (30, 37).

The effect of D643 and E648 mutations on the ion selectivity of the TRPP2_F604P channel was then tested. Three mutations, D643N, D643Q, and E648K, caused significant shifts of current reversal potential in almost all tested ions (Fig. 4*B*). As a result, compared with the TRPP2_F604P channel, the calculated permeability ratio of other ions to $NMDG^+$ (P_X/P_{NMDG}) also changed a lot in these mutant channels (Fig. 4*C* and Table S1). Of these three mutants, D643N had the biggest effect. The reversal potential of TRPP2_F604P_D643N in Na^+ solution shifted from −10.9 mV of TRPP2_F604P to 9.72 mV, in DMA^+ from −16.5 mV to 7.8 mV, and in $Tris^+$ from −27.1 mV to −11.3 mV (Fig. 4*B*, representative currents of D643N are shown in Fig. S5). Correspondingly, calculated P_{Na}/P_{NMDG} changed from 2.5 to 3.3, P_{DMA}/P_{NMDG} changed from 2.0 to 3.0, and P_{TMA}/P_{NMDG} changed from 1.9 to 2.6. (Fig. 4*C* and Table S1). In comparison, another mutation, E648Q, did not cause a significant change in the permeability of any tested ion (Fig. 4 *B* and *C*). From these results, it is reasonable to conclude that D643 is located directly in the channel pore, whereas E648 may not be. However, E648 should be located close to the pore, because a dramatic charge modification at this position (E648K) still causes significant changes in ion selectivity (Fig. 4 *B* and *C* and Table S1).

TRPP2 GOF Channel Serves as a Good Model for Screening the Effects of Pathogenic Mutations on TRPP2 Activity. More than 200 pathogenic TRPP2 mutations have been reported in patients with ADPKD so far (pkd.mayo.edu, by November 2015). Most of the mutations cause truncation in translated TRPP2 proteins. If truncation happens before or within the channel pore forming the S5–S6 transmembrane segments, the resulting TRPP2 should lose channel function. Besides the truncation mutations, there are more than 30 known single- or double-point pathogenic mutations, including deletions and substitutions (pkd.mayo.edu, by November 2015). Studying the effects of these mutations will shed light on the molecular mechanism of TRPP2 function and ADPKD pathogenesis. The GOF TRPP2 serves as a good system for studying these mutants. In the following experiments, nine single- or double-point pathogenic mutations that are spread throughout the TRPP2 protein (Fig. 5*A*) were introduced into the TRPP2_F604P channel, and their effects on channel activity were tested.

Among these nine mutations, R325P (51), W414G (52), and R420G (51) are located in the large extracellular loop between the first and second transmembrane segments (Fig. 5*A*). This extracellular loop is a unique structural feature shared only by the TRPP and TRPML channels in the whole TRP family. The structure and function of this loop are largely unknown. R325 is also part of the conserved polycystin motif that is common in the sequences of almost all TRPP and PKD proteins (53). A recent report showed that W414G abolishes the trafficking of TRPP2 to primary cilium in pig kidney epithelial cells and reduced its single-channel conductance on ER membrane (54). In our experiments, both W414G and R420G abolished or significantly reduced the channel current, whereas R325P had no effect (Fig. 5*B*). The opposite effects of R325P and the other two mutations indicate the multiple roles the extracellular loop plays in TRPP2's function in ADPKD. Next, four pathogenic mutations within the transmembrane regions were tested. Among them, D511V and F605Δ abolished the GOF TRPP2 current as shown earlier in this study (Figs. 2*D* and 5*B*). How D511V affects channel activity is not known, but F605Δ most likely causes conformational changes that lead to the closing of the gate. Two other mutations located in the pore helix, F629S and R638C,

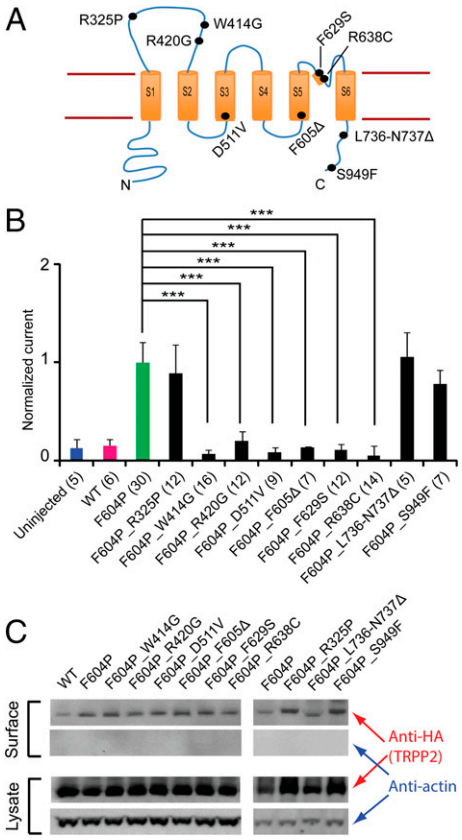

Fig. 5. Effects of ADPKD pathogenic mutations on GOF TRPP2 channel activity. (*A*) Topology of TRPP2 with indicated positions (black dots) of nine pathogenic single- or double-point mutations tested in this study. (*B*) Bar graph showing the effect of the tested pathogenic mutants on TRPP2_F604P current. Currents were recorded in a bath solution containing 100 mM NaCl, 2 mM $CaCl_2$, and 2 mM Hepes-NaOH (pH 7.5). Currents at +60 mV are shown in the bar graph. All currents have been normalized to the average of TRPP2_F604P currents recorded from the same batch of oocytes. Currents of F604P_D511V and F604P_F605Δ are adopted from data in Fig. 2*D*. ***$P < 0.001$. (*C*) Representative Western blot images showing surface expression of the WT TRPP2 channel and channels with indicated mutations. Actin was blotted to show only surface protein detected in the surface protein samples, and serves as a loading control. Statistical analysis on band intensity with data from three independent experiments shows no significant difference in their plasma membrane expression (Fig. S6).

abolished the channel current (Fig. 5*B*), indicating that the proper conformation in this region is crucial for ion permeability. Furthermore, two pathogenic mutations located at the C terminus of TRPP2 were tested. Introduction of the double-point deletion mutation L736-N737Δ in the EF-hand motif caused no change on the channel current (Fig. 5*B*). Similarly, a substitution mutation S949F (pkdb.mayo.edu), located 20 amino acids upstream of the carboxyl terminus of TRPP2, also caused no change in the TRPP2_F604P current (Fig. 5*B*). All of the tested pathogenic mutations expressed on oocyte plasma membrane as WT and F604P channels (Fig. 5*C* and Fig. S6), indicating that trafficking is not the reason why some of these mutations abolish TRPP2_F604P current.

GOF TRPP2 Functions Better in Rescuing the Defects of Zebrafish Embryos Induced by Knocking Down the Endogenous TRPP2. Loss of function of TRPP2 induces ADPKD in humans. Therefore, restoration of TRPP2 function has potential value in the development of therapeutic strategies. This restoration strategy has been shown to be virtually effective in zebrafish, a widely used animal model for ADPKD and TRPP2 study (55–59). Knocking down TRPP2 in zebrafish embryos with morpholino (MO) oligos resulted in cyst formation in the pronephric kidney and dorsal axis curvature (curly tail) (55). Both phenotypes can be rescued by injecting human TRPP2 RNA into one- to two-cell-stage fish embryos (56, 57). Although there is no direct evidence, injected TRPP2 RNA most likely rescues the MO-induced defects by restoring TRPP2 channel activity. If this assumption is true, we can then hypothesize that the GOF TRRP2, which has more channel activity than WT, will rescue the MO-induced defects more efficiently.

In our experiment, after MO directed against zebrafish TRPP2 was injected into one-cell embryos, the fish embryos exhibited a curly tail phenotype with variable severity at 48 hours post-fertilization (hpf) (Fig. 6*A*). Based on the severity of curly tail, fish were divided into four categories as previously reported (60): normal (no curvature), mild (<90°), moderate (>90°), and severe (tail tip crossing the body axis) (Fig. 6*A*). It has been reported that the curly tail phenotype correlates with cyst formation in the pronephric kidney of zebrafish (55, 56). In this study, the relationship between the severity of the curly tail phenotype and the kidney cyst formation was quantitatively analyzed with the *wt1b:EGFP* transgenic fish line [Tg(wt1b:eGFP)^{li1}] (61). These fish express GFP specifically in their pronephric kidney, which makes it possible to monitor the cyst formation by measuring the size of the glomerulus under GFP fluorescence (Fig. 6 *C* and *D*). An oversized glomerulus indicates cyst formation. Our results show a strong correlation between the severity of the curly tail phenotype and the glomerulus size (Fig. 6*E*). The more severe the curly tail, the bigger were the glomeruli/cysts. Cyst formation in the oversized glomerulus in zebrafish embryos with severe curly tail was further confirmed by reconstructed 3D structures with confocal images of the glomerulus (Fig. S7). These results confirm that the severity of cystogenesis in the pronephric kidney can be judged by monitoring the severity of the curly tail phenotype.

After coinjecting 50 pg of human TRPP2 RNA with MO, the overall severity of curly tail became significantly lower than in the MO-only injected group (Fig. 6*B*, *Left*, second and third bars on the graph). Compared with 80% of the MO-only injected group, less than 40% of embryos had either moderate or severe curly tail in the MO + TRPP2 RNA-injected group (Fig. 6*B*). Significantly better rescue was observed in the group of embryos injected with MO and 50 pg of TRPP2_F604P RNA; only 24% of fish had either moderate or severe curly tail (Fig. 6*B*, *Left*, fourth bar on the graph). Compared with 13% in the WT TRPP2-injected group, 46% of fish had a normal body dorsal axis in the TRPP2_F604P-injected group (Fig. 6*B* and Fig. S8*A*). No clear difference was found in the expression level of these two proteins in zebrafish (Fig. S8*B*). These results indicate that TRPP2_F604P rescues the dorsal axis curvature better than WT TRPP2. Because the main difference between the TRPP2_F604P and the WT channel is the constitutive channel activity of TRPP2_F604P, our results strongly suggest that TRPP2 rescues the curly tail phenotype and cystogenesis by means of its ion channel activity, and that our GOF TRPP2 has higher activity than the WT channel in vivo. Consistently, the rescue effect was abolished by introducing a loss-of-function pathogenic mutation, D511V, into the TRPP2_F604P (Fig. 6*B*, *Right*), while protein expression in zebrafish was not affected (Fig. S8*B*). This result is consistent with a previous finding that TRPP2 RNA with the D511V mutation failed in rescuing MO-induced defects in zebrafish (58).

Discussion

Although the TRPP2 ion channel plays a crucial role in cell signaling in renal and nonrenal cells, study on its function and regulation is limited by the lack of a suitable system for recording its channel activity. In the present study, by performing systematic mutagenesis on the S4–S5 linker and the first half of S5, we found that a single mutation, F604P, on S5 causes constitutive

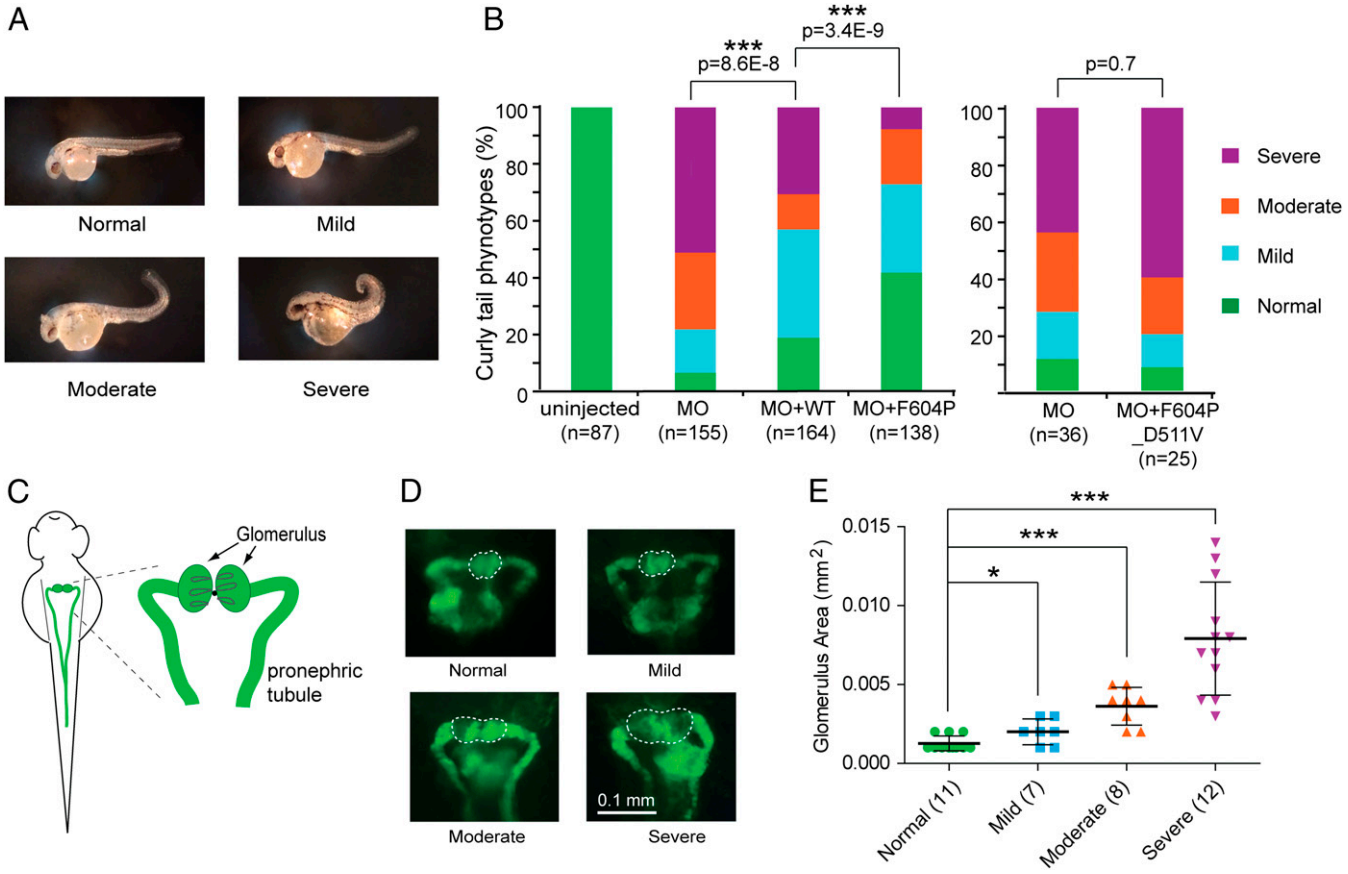

Fig. 6. GOF TRPP2 rescues the dorsal axis curvature (curly tail) phenotype in zebrafish embryos better than WT TRPP2. (*A*) Representative images of zebrafish embryos showing the range of severity in curly tail used for scoring. Normal: no curvature; mild: <90°; moderate: >90°; severe: tail tip crossing the body axis. (*B*) Bar graph represents the percentage of embryos with normal, mild, moderate, and severe curvature at 48 hpf. Embryos were injected at the one-cell stage with zebrafish TRPP2 MO or indicated combinations of MO and RNA. Statistical significance is determined by the χ^2 test. Data used in the *Left* bar graph were pooled from five independent experiments, whereas data used in the *Right* bar graph were pooled from two experiments. (*C*) Diagram showing fish pronephric kidney at around 48 hpf. (*Right*) Glomerulus and pronephric tubule are labeled on the zoom-in diagram. (*D*) Representative fluorescence images showing the area of the glomerulus (circled with dashed lines) of zebrafish embryos with different severity in dorsal axis curvature as shown in *A*. The transgenic line *wt1b:EGFP* [Tg(wt1b:eGFP)^{li1}] with pronephros-specific GFP expression was used in this experiment. (*E*) Scatter plot showing the correlation between glomerulus area and indicated curly tail severity. The glomerulus area was selected as shown with the dashed lines in *D*, and was measured with ImageJ. The mean and SD are indicated in the plot. *$P < 0.05$; ***$P < 0.001$.

opening of TRPP2 (Fig. 1). The overall structures of TRP channels are similar to the overall structures of voltage-gated cation channels, such as the voltage-gated potassium channel (Kv) (62, 63). In the Kv channel, the S4–S5 linker helix couples the movement of the voltage sensor in S4 to channel gating through the interaction between the S4–S5 linker, S5, and S6 (64). Similar local structural features have been found in TRPV1 (63), TRPV2 (65), and TRPA1 (66), indicating that a common gating mechanism exists between the Kv and TRP channels. The role that the S4–S5 linker plays in the gating of the TRPV4 channel was recently explained by a homology model of this channel (67). In this model, L596, an amino acid on the S4–S5 linker, interacts with W733 in the C-terminal TRP domain to lock the channel in its closed state (67). The TRP domain is a highly conserved region in most TRP channels, located right after S6 (68). Consistently, the GOF mutants of TRP channels found in diseases and random mutagenesis studies showed that large hydrophobic amino acids, especially Phe, in the S4–S5 linker and the first half of S5 play a crucial role in keeping TRP channels in the closed state (35). Changing these amino acids may lead to constitutive activation of the channels (35). Compared with other TRP members, TRPP proteins do not contain the TRP domain (68), and, so far, there is no report of a GOF mutation in the S4–S5 linker or S5 of any TRPP channels. Our results with TRPP2_F604P indicate, for the first time to our knowledge, that TRPP channels share a similar gating mechanism with other TRPs even though the conserved TRP domain is missing.

Ca^{2+} is an important regulator of TRPP channel activity. Previous studies showed that extracellular Ca^{2+} inhibits channel currents carried by monovalent cations in both the TRPP2 and TRPP3 channels (19, 20, 37, 43). Meanwhile, TRPP2 activity is regulated by cytoplasmic Ca^{2+} concentration in a bell-shaped manner. Applying Ca^{2+} below micromolar concentrations on the cytoplasmic side increases channel activity, but a higher concentration of Ca^{2+} inhibits the channel activity (20, 21, 29). In our experiments, application of extracellular Ca^{2+}, Mg^{2+}, or Ba^{2+} abolished most of the inward current of TRPP2_F604P carried by the monovalent ion Na^+ (Fig. 3 *C*–*H* and Fig. S3). The voltage dependence of divalent blocking in TRPP2_F604P indicates an open-channel blocking mechanism (Fig. 3 *D*, *E*, *G*, and *H*). Depolarization removes the divalent ions from their binding site in the pore and releases the blocking.

Ca^{2+} blocking plays important roles in the function of Ca^{2+}-permeable channels. In these channels, Ca^{2+} must first bind to a site inside the pore to permeate. Thus, the ability of divalent ions, such as Ca^{2+}, to block the monovalent ion current is pretty

common in these channels. Some very well-studied examples are the voltage-gated calcium channel (69), CNG channel in vertebrate photoreceptors (47), and TRPL channel in fly photoreceptors (70). In all cases, Ca^{2+} binds to the pore and blocks the current carried by monovalent ions in a voltage-dependent manner. The fact that Ca^{2+} functions as an open-channel blocker of the TRPP2_F604P channel indicates that Ca^{2+} has high binding affinity in the channel pore of TRPP2. It also indicates that the TRPP2 channel is normally blocked in physiological conditions when millimolar Ca^{2+} and negative membrane potential exist. In the CNG and TRPL channels, Ca^{2+} blocking is thought to limit Ca^{2+} influx when intense signal (light) exists and plays a crucial role in reducing the noise level and adapting to intense signals (70, 71). It will be very interesting to find out how much Ca^{2+} influx through TRPP2 happens under blocking conditions and what role Ca^{2+} blocking plays in the function of TRPP2 in vivo.

A recent study showed that cell cilia function as an independent calcium compartment and the calcium concentration change in cilia is isolated from the calcium concentration change in the cell cytoplasm (72). Because the volume of cilium is very small (~0.5 fL), a tiny influx of Ca^{2+} ions is enough to bring the calcium concentration to a significant level to induce the signaling in cilia (72). If TRPP2 indeed functions as a Ca^{2+}-permeable channel on ciliary membrane, then a large Ca^{2+} influx through TRPP2 may not be necessary. Therefore, the extracellular divalent ion inhibition may function in vivo to prevent excessive influx of Ca^{2+} through TRPP2. Consistent with this hypothesis, currents recorded from the TRPP3/PKD1L1 complex on ciliary membrane showed strong outward rectification in Ca^{2+}-containing bath solutions, indicating the possibility of also having similar divalent ion blocking properties (73).

Our GOF TRPP2 is a very useful tool in studying TRPP2 function and regulation. Its application was demonstrated in this study by analyzing the effects of native pathogenic mutations (Fig. 5). Results showed that although most of the tested mutations, including the ones in the I–II loop, transmembrane segments, and pore region, abolish or greatly reduce channel activity, one mutation in the extracellular I–II loop and two mutations in the C terminus did not affect the channel current (Fig. 5*B*). These mutations may cause ADPKD by affecting trafficking or regulation of TRPP2, or its association with other binding partners (thus disrupting the downstream signaling pathway). Although more studies need to be done to clarify further the effects of these current-abolishing and non–current-abolishing mutations, our results indicate that different pathogenic mutations have varying effects on TRPP2 channel activity and may lead to different subtypes of ADPKD. Thus, corresponding therapeutic strategies have to be developed to treat patients with different pathogenic mutations.

The C terminus is crucial for the function of TRPP2 in many areas, including assembly with polycystin-1 (7–9); interaction with other partners, such as TRPC1 (74); subcellular localization (25); and channel activity regulation (21, 29). The C terminus of TRPP2 is also involved in association with cytoskeletal proteins, such as actin and filamin, which have been shown to regulate the stability, trafficking, and channel function of TRPP2 (75, 76). However, in this current study, two mutations in the C terminus were found to have no effect on GOF TRPP2 channel activity (Fig. 5*B*). L736 and N737 are located in the C-terminal EF-hand motif, a domain involved in Ca^{2+} regulation of TRPP2 activity (77–80). Although they are not directly involved in Ca^{2+} binding (78), deletion of L736 and N737 most likely alters Ca^{2+} regulation by deforming the Ca^{2+} binding site. Previous study has shown that the mutation L736-N737Δ changed the response of TRPP2 to cytosolic Ca^{2+} (78). However, because Ca^{2+} regulation on channel gating is most likely missing in the constitutively open GOF channel, it is not a surprise to see that L736-N737Δ did not affect the GOF channel current (Fig. 5*B*). The second mutant, S949F, also has no effect on channel activity (Fig. 5*B*), indicating a possible role of S949 in other crucial functions of TRPP2, such as interacting with downstream signal molecules or cytoskeletal proteins. A previous report showed that the disease-causing truncation mutation TRPP2_R742X, which misses most of the C terminus, forms a functional channel on the plasma membrane (37). Together, these results indicate the C terminus is not necessary for TRPP2 ion channel activity, although it plays crucial roles in regulating the function of TRPP2 as mentioned above.

Our zebrafish experiment showed that compared with WT TRPP2, GOF TRPP2 better rescued zebrafish defects (curly tail and kidney cysts) caused by down-regulation of endogenous TRPP2 expression (Fig. 6). These data strongly suggest that rescue of these defects benefits from the higher channel activity of the GOF TRPP2. In a recent study, it was shown that the restoration of human TRPP2 expression/function significantly rescued ADPKD phenotypes in a TRPP2 KO mouse model in a dose-dependent manner (81). Together with our results, the current evidence indicates that elevation of TRPP2 activity may be helpful for ADPKD treatment. It is crucial to figure out further how TRPP2 activity rescues ADPKD phenotypes. Because TRPP2 channel function has been described both in the presence (12, 13, 18) and absence of polycystin-1 (19–21), it will be very interesting to find out whether polycystin-1 is involved in the rescue caused by TRPP2 activity. Also, TRPP2 has been shown to be localized on multiple subcellular compartments and may have distinct functions in each compartment (3, 22–24). Therefore, it is also important to find out how temporal and spatial regulation of TRPP2 function contributes to the rescuing.

ADPKD is caused by mutations in either polycystin-1 or TRPP2. Because mutations in these two proteins produce similar pathological manifestations and they assemble as a complex (7–10), polycystin-1 and TRPP2 are proposed to participate in the same molecular and cellular process. It is generally believed that in the TRPP2/polycystin-1 complex, polycystin-1 is the receptor that detects extracellular signals, such as fluid flow (13), and opens the TRPP2 channel to conduct Ca^{2+} influx (11). Our results in zebrafish indicated that GOF TRPP2 has higher basal channel activity in vivo than the WT (Fig. 6). Thus, a GOF TRPP2 with its constitutive activity has the potential to bypass the initial signal acceptance and conduct the Ca^{2+} influx directly. In other words, the GOF TRPP2 may be able to compensate for the functional loss of TRPP2/polycystin-1 complex, regardless of whether the mutation is on polycystin-1 or TRPP2. Therefore, in addition to serving as a useful tool for studying the function, regulation, and pharmacology of TRPP2, the GOF TRPP2 may be valuable in developing new therapeutic strategies for ADPKD. It is necessary to further evaluate its therapeutic application with ADPKD mouse models.

Materials and Methods

cDNA Constructs and Cloning. Human TRPP2 cDNAs (National Center for Biotechnology Information accession no. U50928) were cloned into a modified pGEMHE vector for in vitro transcription. Mutations were introduced by PCR, and all constructs were verified by sequencing. Unless otherwise indicated, the DNA sequence of an HA epitope tag was added to the 5′ end of TRPP2 cDNA to generate N-terminal HA-tagged TRPP2.

Electrophysiology. TEVC experiments were performed as described previously (49). In brief, cRNAs were synthesized in vitro and injected into follicle membrane free oocytes (50 ng of cRNA per oocyte). After injection, the oocytes were incubated at 18 °C for 3 to 4 d before whole-oocyte currents were recorded. Unless otherwise indicated, whole-cell currents of oocytes were recorded at room temperature in standard divalent ion-free bath solution [containing 100 mM NaCl, 2 mM Hepes (pH 7.5)] or Ca^{2+}-containing bath solution [100 mM NaCl, 2 mM $CaCl_2$, 2 mM Hepes (pH 7.5)]. A standard TEVC protocol includes holding oocytes at −60 mV and measuring the current-voltage (I-V) relationships by applying 50-ms voltage steps from −80 to +60 mV in 10-mV increments.

For the Ab blocking experiments in Fig. 2*B*, oocytes were first held at −60 mV and perfused with standard divalent ion-free bath solution. Perfusion was stopped, and 50 μg/mL mouse monoclonal anti-TRPP2 Ab that recognizes aa 261–360 in the extracellular loop of TRPP2 (LifeSpan Biosciences) or 50 μg/mL mouse monoclonal anti-GFP Ab (Santa Cruz Biotechnology) was applied drop-wise onto oocytes for 20 s.

In the experiments for determining ion permeability, oocytes were perfused with standard divalent ion-free bath solution first, and the voltage step protocol was applied to extract the I-V curve and the reversal potential of Na^+. Oocytes were then washed with solutions in which 100 mM NaCl was replaced with 100 mM KCl, LiCl, RbCl, CsCl, DMA hydrochloride, TMA hydrochloride, Tris·HCl, or NMDG-HCl. The I-V was monitored with a voltage ramps protocol (from −70 to +60 mV in 160 ms) until the reversal potential shift stopped (usually takes about 20 s). Finally, another voltage step protocol was applied to extract the I-V curve and reversal potential for the tested ion. Relative permeability of the tested ions was calculated based on the difference between the reversal potential of the tested ion and Na^+ (Fig. 1*D*) or $NMDG^+$ (Fig. 4). The permeability ratios, for example, P_X/P_{NMDG}, were calculated using the following Goldmann–Hodgkin–Katz equation (82):

$$P_X/P_{NMDG} = e^{\Delta E_{rev} F/RT},$$

where E_{rev} is the reversal potential and ΔE_{rev} is the shift of reversal potential when ion X^+ was switched to $NMDG^+$. $\Delta E_{rev} = E_{rev,X} - E_{rev,NMDG}$. F is Faraday's constant, R is the universal gas constant, and T is the absolute temperature.

Data of electrophysiology experiments are presented as mean values ± SD. Statistical significance is determined by an unpaired, two-tailed Student's *t* test.

Surface Protein Biotinylation. Proteins on *Xenopus* oocyte plasma membrane were detected with a Pierce Cell Surface Protein Isolation Kit by following a slightly modified protocol as described previously (83). In brief, 3 or 4 d after cRNA injection, oocytes (20 oocytes per reaction) were washed with ice-cold calcium-free oocyte Ringer's solution (OR2) [82.4 mM NaCl, 2.5 mM KCl, 1 mM $MgCl_2$, 10 mM Hepes (pH 7.6)]. Oocytes were then incubated with 1.2 mg/mL sulfo-NHS-SS-biotin in OR2 at 4 °C for 30 min. The reaction was quenched, and oocytes were washed following the manufacturer's protocol. Oocytes were then homogenized and lysed. Lysates were mixed with streptavidin magnetic beads at 4 °C overnight. After beads were washed, proteins were eluted with SDS sample loading buffer with DTT at 37 °C for 30 min. Eluted samples were analyzed with SDS/PAGE and Western blot. Relative intensity of Western blot bands was measured with ImageJ (NIH) and analyzed with Student's *t* test.

SDS/PAGE and Western Blotting. Western blot analysis was performed as described previously (49). Protein samples were run on 4–12% Bolt Bis-Tris Plus gels (Life Technologies) and transferred to a PVDF membrane. Mouse monoclonal anti-HA (BioLegend) or anti–β-actin Ab (GenScript) was used. Blot signals were visualized with a Molecular Imager Chemi Doc XRS+ imaging system (Bio-Rad).

MO and mRNA Injection in Zebrafish. WT or *wt1b:EGFP* transgenic [Tg(wt1b:eGFP)^{li1}] (61) zebrafish were maintained at 28 °C on a 14-h/10-h light/dark (regular) cycle. Embryos were collected from natural breeding and selected by developmental and morphological criteria.

Zebrafish TRPP2 MO oligos were ordered from Gene Tools. The MO oligo (sequence: 5-AGGACGAACGCGACTGGAGCTCATC-3) was designed previously (55) to inhibit translation of the corresponding zebrafish TRPP2 gene. To knock down endogenous zebrafish TRPP2, embryos of WT or *wt1b:EGFP* transgenic line fish at the one-cell stage were microinjected with 0.25 mM antisense MO oligos in 100 mM KCl and 0.5% Phenol Red with a volume of 500 pL per embryo. In rescue experiments, 50 pg of in vitro synthesized human TRPP2 cRNA (WT or mutant) was injected, together with 0.25 mM MO. Embryos from the same clutch with the same parents were used for injection when direct comparison was made within groups. MO- and RNA-injected embryos were incubated at 28 °C and observed for phenotypes at 48 hpf. Statistical significance between groups was determined by the χ^2 test.

To prepare samples for Western blot to show the expression of HA-tagged human WT and mutant TRPP2 in zebrafish, 60 fish at 48 hpf were collected from each group and lysed with lysis solution containing 1% *n*-Dodecyl β-D-maltoside, 5 mM EDTA, and protease inhibitor mixture (Pierce). HA-tagged TRPP2 proteins were then pulled down from fish lysate with anti-HA Ab-coated magnetic beads (Pierce) following the protocol from the manufacturer. Proteins were analyzed by Western blot with mouse monoclonal anti-HA Ab (BioLegend).

Zebrafish Image Acquisition. The pronephros, identified in the Tg(wt1b:eGFP)^{li1} as GFP-positive, was imaged using a fluorescence microscope (Zeiss SteREO Discovery V12) with a camera (Zeiss AxioCam MRc). The area of glomerulus was measured from the GFP-positive regions using ImageJ (NIH). The scale was set in ImageJ with an image of a micrometer and used to calculate the glomerulus area. Statistical significance was determined by the Student's *t* test. For confocal imaging, briefly, Tg(wt1b:eGFP)^{li1} embryos, immobilized with tricaine and screened for GFP expression at 48 hpf, were mounted in 2% low-melt agarose on a glass-bottomed dish with the pronephros positioned directly adjacent to the coverslip. The embryos were then imaged under the 20× objective on an inverted Leica SP5 spectral confocal microscope. Three-dimensional reconstructions of GFP expression were rendered in Imaris (Bitplane, USA).

Animal Use. All frogs and zebrafish care and experimental protocols were conducted upon approval of the Institutional Animal Care and Use Committee of St. John's University; Yale University; and Queens College, City University of New York.

ACKNOWLEDGMENTS. We thank Dr. Yiqiang Cai (Yale University) for human TRPP2 cDNA and Dr. Christoph Englert (Leibniz Institute on Aging) for the Tg(wt1b:eGFP)^{li1} line of fish. We thank Marie Birne and Arelys Uribe for managing the fish facility and Corinna Singleman and Sana Khan for help on zebrafish experiments (Queens College). We thank Fangyong Li (Yale University) for help on statistics, Dr. Lawrence Pamler (Cornell University) for help on experimental design, and Lu Xu (Columbia University) for technical support. We thank members of the Y.Y. laboratory for commenting on the manuscript. Some of the imaging experiments were performed at the Core Faculties for Imaging, Cellular and Molecular Biology (Queens College). This work was supported by NIH Grants DK102092 (to Y.Y.) and EY021195 (to D.Z.).

1. Harris PC, Torres VE (2009) Polycystic kidney disease. *Annu Rev Med* 60:321–337.
2. Wu G, Somlo S (2000) Molecular genetics and mechanism of autosomal dominant polycystic kidney disease. *Mol Genet Metab* 69(1):1–15.
3. Semmo M, Köttgen M, Hofherr A (2014) The TRPP subfamily and polycystin-1 proteins. *Handbook Exp Pharmacol* 222:675–711.
4. Hughes J, et al. (1995) The polycystic kidney disease 1 (PKD1) gene encodes a novel protein with multiple cell recognition domains. *Nat Genet* 10(2):151–160.
5. Mochizuki T, et al. (1996) PKD2, a gene for polycystic kidney disease that encodes an integral membrane protein. *Science* 272(5266):1339–1342.
6. Ramsey IS, Delling M, Clapham DE (2006) An introduction to TRP channels. *Annu Rev Physiol* 68:619–647.
7. Qian F, et al. (1997) PKD1 interacts with PKD2 through a probable coiled-coil domain. *Nat Genet* 16(2):179–183.
8. Tsiokas L, Kim E, Arnould T, Sukhatme VP, Walz G (1997) Homo- and heterodimeric interactions between the gene products of PKD1 and PKD2. *Proc Natl Acad Sci USA* 94(13):6965–6970.
9. Yu Y, et al. (2009) Structural and molecular basis of the assembly of the TRPP2/PKD1 complex. *Proc Natl Acad Sci USA* 106(28):11558–11563.
10. Zhu J, et al. (2011) Structural model of the TRPP2/PKD1 C-terminal coiled-coil complex produced by a combined computational and experimental approach. *Proc Natl Acad Sci USA* 108(25):10133–10138.
11. Zhou J (2009) Polycystins and primary cilia: Primers for cell cycle progression. *Annu Rev Physiol* 71:83–113.
12. Hanaoka K, et al. (2000) Co-assembly of polycystin-1 and -2 produces unique cation-permeable currents. *Nature* 408(6815):990–994.
13. Nauli SM, et al. (2003) Polycystins 1 and 2 mediate mechanosensation in the primary cilium of kidney cells. *Nat Genet* 33(2):129–137.
14. McGrath J, Somlo S, Makova S, Tian X, Brueckner M (2003) Two populations of node monocilia initiate left-right asymmetry in the mouse. *Cell* 114(1):61–73.
15. Pennekamp P, et al. (2002) The ion channel polycystin-2 is required for left-right axis determination in mice. *Curr Biol* 12(11):938–943.
16. Kamura K, et al. (2011) Pkd1l1 complexes with Pkd2 on motile cilia and functions to establish the left-right axis. *Development* 138(6):1121–1129.
17. Field S, et al. (2011) Pkd1l1 establishes left-right asymmetry and physically interacts with Pkd2. *Development* 138(6):1131–1142.
18. Delmas P, et al. (2004) Gating of the polycystin ion channel signaling complex in neurons and kidney cells. *FASEB J* 18(6):740–742.
19. González-Perrett S, et al. (2001) Polycystin-2, the protein mutated in autosomal dominant polycystic kidney disease (ADPKD), is a Ca2+-permeable nonselective cation channel. *Proc Natl Acad Sci USA* 98(3):1182–1187.
20. Vassilev PM, et al. (2001) Polycystin-2 is a novel cation channel implicated in defective intracellular Ca(2+) homeostasis in polycystic kidney disease. *Biochem Biophys Res Commun* 282(1):341–350.
21. Koulen P, et al. (2002) Polycystin-2 is an intracellular calcium release channel. *Nat Cell Biol* 4(3):191–197.

22. Giamarchi A, et al. (2006) The versatile nature of the calcium-permeable cation channel TRPP2. *EMBO Rep* 7(8):787–793.
23. Köttgen M (2007) TRPP2 and autosomal dominant polycystic kidney disease. *Biochim Biophys Acta* 1772(8):836–850.
24. Tsiokas L, Kim S, Ong EC (2007) Cell biology of polycystin-2. *Cell Signal* 19(3):444–453.
25. Cai Y, et al. (1999) Identification and characterization of polycystin-2, the PKD2 gene product. *J Biol Chem* 274(40):28557–28565.
26. Luo Y, Vassilev PM, Li X, Kawanabe Y, Zhou J (2003) Native polycystin 2 functions as a plasma membrane Ca2+-permeable cation channel in renal epithelia. *Mol Cell Biol* 23(7):2600–2607.
27. Ma R, et al. (2005) PKD2 functions as an epidermal growth factor-activated plasma membrane channel. *Mol Cell Biol* 25(18):8285–8298.
28. Pelucchi B, et al. (2006) Nonspecific cation current associated with native polycystin-2 in HEK-293 cells. *J Am Soc Nephrol* 17(2):388–397.
29. Cai Y, et al. (2004) Calcium dependence of polycystin-2 channel activity is modulated by phosphorylation at Ser812. *J Biol Chem* 279(19):19987–19995.
30. Anyatonwu GI, Ehrlich BE (2005) Organic cation permeation through the channel formed by polycystin-2. *J Biol Chem* 280(33):29488–29493.
31. Ćelić AS, et al. (2012) Calcium-induced conformational changes in C-terminal tail of polycystin-2 are necessary for channel gating. *J Biol Chem* 287(21):17232–17240.
32. Wang Q, et al. (2012) Structural interaction and functional regulation of polycystin-2 by filamin. *PLoS One* 7(7):e40448.
33. Gonzalez-Perrett S, et al. (2002) Voltage dependence and pH regulation of human polycystin-2-mediated cation channel activity. *J Biol Chem* 277(28):24959–24966.
34. Xu GM, et al. (2003) Polycystin-1 activates and stabilizes the polycystin-2 channel. *J Biol Chem* 278(3):1457–1462.
35. Myers BR, Saimi Y, Julius D, Kung C (2008) Multiple unbiased prospective screens identify TRP channels and their conserved gating elements. *J Gen Physiol* 132(5): 481–486.
36. Dong XP, et al. (2009) Activating mutations of the TRPML1 channel revealed by proline-scanning mutagenesis. *J Biol Chem* 284(46):32040–32052.
37. Chen XZ, et al. (2001) Transport function of the naturally occurring pathogenic polycystin-2 mutant, R742X. *Biochem Biophys Res Commun* 282(5):1251–1256.
38. Reynolds DM, et al. (1999) Aberrant splicing in the PKD2 gene as a cause of polycystic kidney disease. *J Am Soc Nephrol* 10(11):2342–2351.
39. Garcia-Gonzalez MA, et al. (2007) Evaluating the clinical utility of a molecular genetic test for polycystic kidney disease. *Mol Genet Metab* 92(1-2):160–167.
40. Jordt SE, Julius D (2002) Molecular basis for species-specific sensitivity to "hot" chili peppers. *Cell* 108(3):421–430.
41. Voets T, et al. (2002) Molecular determinants of permeation through the cation channel TRPV4. *J Biol Chem* 277(37):33704–33710.
42. Köttgen M, et al. (2008) TRPP2 and TRPV4 form a polymodal sensory channel complex. *J Cell Biol* 182(3):437–447.
43. Chen XZ, et al. (1999) Polycystin-L is a calcium-regulated cation channel permeable to calcium ions. *Nature* 401(6751):383–386.
44. Schroeder BC, Cheng T, Jan YN, Jan LY (2008) Expression cloning of TMEM16A as a calcium-activated chloride channel subunit. *Cell* 134(6):1019–1029.
45. Miledi R (1982) A calcium-dependent transient outward current in Xenopus laevis oocytes. *Proc R Soc Lond B Biol Sci* 215(1201):491–497.
46. Barish ME (1983) A transient calcium-dependent chloride current in the immature Xenopus oocyte. *J Physiol* 342:309–325.
47. Seifert R, Eismann E, Ludwig J, Baumann A, Kaupp UB (1999) Molecular determinants of a Ca2+-binding site in the pore of cyclic nucleotide-gated channels: S5/S6 segments control affinity of intrapore glutamates. *EMBO J* 18(1):119–130.
48. Shimizu T, Janssens A, Voets T, Nilius B (2009) Regulation of the murine TRPP3 channel by voltage, pH, and changes in cell volume. *Pflugers Arch* 457(4):795–807.
49. Yu Y, et al. (2012) Molecular mechanism of the assembly of an acid-sensing receptor ion channel complex. *Nat Commun* 3:1252.
50. Fujimoto C, et al. (2011) The single pore residue Asp523 in PKD2L1 determines Ca2+ permeation of the PKD1L3/PKD2L1 complex. *Biochem Biophys Res Commun* 404(4): 946–951.
51. Stekrová J, et al. (2004) PKD2 mutations in a Czech population with autosomal dominant polycystic kidney disease. *Nephrol Dial Transplant* 19(5):1116–1122.
52. Veldhuisen B, et al. (1997) A spectrum of mutations in the second gene for autosomal dominant polycystic kidney disease (PKD2). *Am J Hum Genet* 61(3):547–555.
53. Li A, Tian X, Sung SW, Somlo S (2003) Identification of two novel polycystic kidney disease-1-like genes in human and mouse genomes. *Genomics* 81(6):596–608.
54. Cai Y, et al. (2014) Altered trafficking and stability of polycystins underlie polycystic kidney disease. *J Clin Invest* 124(12):5129–5144.
55. Sun Z, et al. (2004) A genetic screen in zebrafish identifies cilia genes as a principal cause of cystic kidney. *Development* 131(16):4085–4093.
56. Obara T, et al. (2006) Polycystin-2 immunolocalization and function in zebrafish. *J Am Soc Nephrol* 17(10):2706–2718.
57. Streets AJ, Moon DJ, Kane ME, Obara T, Ong AC (2006) Identification of an N-terminal glycogen synthase kinase 3 phosphorylation site which regulates the functional localization of polycystin-2 in vivo and in vitro. *Hum Mol Genet* 15(9):1465–1473.
58. Feng S, et al. (2008) Identification and functional characterization of an N-terminal oligomerization domain for polycystin-2. *J Biol Chem* 283(42):28471–28479.
59. Giamarchi A, et al. (2010) A polycystin-2 (TRPP2) dimerization domain essential for the function of heteromeric polycystin complexes. *EMBO J* 29(7):1176–1191.
60. Mangos S, et al. (2010) The ADPKD genes pkd1a/b and pkd2 regulate extracellular matrix formation. *Dis Model Mech* 3(5-6):354–365.
61. Perner B, Englert C, Bollig F (2007) The Wilms tumor genes wt1a and wt1b control different steps during formation of the zebrafish pronephros. *Dev Biol* 309(1):87–96.
62. Long SB, Tao X, Campbell EB, MacKinnon R (2007) Atomic structure of a voltage-dependent K+ channel in a lipid membrane-like environment. *Nature* 450(7168): 376–382.
63. Liao M, Cao E, Julius D, Cheng Y (2013) Structure of the TRPV1 ion channel determined by electron cryo-microscopy. *Nature* 504(7478):107–112.
64. Long SB, Campbell EB, Mackinnon R (2005) Voltage sensor of Kv1.2: Structural basis of electromechanical coupling. *Science* 309(5736):903–908.
65. Zubcevic L, et al. (2016) Cryo-electron microscopy structure of the TRPV2 ion channel. *Nat Struct Mol Biol* 23(2):180–186.
66. Paulsen CE, Armache JP, Gao Y, Cheng Y, Julius D (2015) Structure of the TRPA1 ion channel suggests regulatory mechanisms. *Nature* 525(7570):552.
67. Teng J, Loukin SH, Anishkin A, Kung C (2015) L596-W733 bond between the start of the S4-S5 linker and the TRP box stabilizes the closed state of TRPV4 channel. *Proc Natl Acad Sci USA* 112(11):3386–3391.
68. Montell C (2005) The TRP superfamily of cation channels. *Sci STKE* 2005(272):re3.
69. Yang J, Ellinor PT, Sather WA, Zhang JF, Tsien RW (1993) Molecular determinants of Ca2+ selectivity and ion permeation in L-type Ca2+ channels. *Nature* 366(6451): 158–161.
70. Parnas M, Katz B, Minke B (2007) Open channel block by Ca2+ underlies the voltage dependence of drosophila TRPL channel. *J Gen Physiol* 129(1):17–28.
71. Kaupp UB, Seifert R (2002) Cyclic nucleotide-gated ion channels. *Physiol Rev* 82(3): 769–824.
72. Delling M, DeCaen PG, Doerner JF, Febvay S, Clapham DE (2013) Primary cilia are specialized calcium signalling organelles. *Nature* 504(7479):311–314.
73. DeCaen PG, Delling M, Vien TN, Clapham DE (2013) Direct recording and molecular identification of the calcium channel of primary cilia. *Nature* 504(7479):315–318.
74. Tsiokas L, et al. (1999) Specific association of the gene product of PKD2 with the TRPC1 channel. *Proc Natl Acad Sci USA* 96(7):3934–3939.
75. Chen XZ, et al. (2008) Submembraneous microtubule cytoskeleton: Interaction of TRPP2 with the cell cytoskeleton. *FEBS J* 275(19):4675–4683.
76. Wang Q, et al. (2015) Filamin-a increases the stability and plasma membrane expression of polycystin-2. *PLoS One* 10(4):e0123018.
77. Cantiello HF (2004) Regulation of calcium signaling by polycystin-2. *Am J Physiol Renal Physiol* 286(6):F1012–F1029.
78. Petri ET, et al. (2010) Structure of the EF-hand domain of polycystin-2 suggests a mechanism for Ca2+-dependent regulation of polycystin-2 channel activity. *Proc Natl Acad Sci USA* 107(20):9176–9181.
79. Schumann F, et al. (2009) Ca2+-dependent conformational changes in a C-terminal cytosolic domain of polycystin-2. *J Biol Chem* 284(36):24372–24383.
80. Kuo IY, et al. (2014) The number and location of EF hand motifs dictates the calcium dependence of polycystin-2 function. *FASEB J* 28(5):2332–2346.
81. Li A, et al. (2015) Human polycystin-2 transgene dose-dependently rescues ADPKD phenotypes in Pkd2 mutant mice. *Am J Pathol* 185(10):2843–2860.
82. Hille B (2001) *Ion Channels of Excitable Membranes* (Sinauer, Sunderland, MA), 3rd Ed.
83. Pavel MA, et al. (2014) Analysis of the cell surface expression of cytokine receptors using the surface protein biotinylation method. *Methods Mol Biol* 1172:185–192.
84. Hong YS, et al. (2002) Single amino acid change in the fifth transmembrane segment of the TRP Ca2+ channel causes massive degeneration of photoreceptors. *J Biol Chem* 277(37):33884–33889.
85. Becker EB, et al. (2009) A point mutation in TRPC3 causes abnormal Purkinje cell development and cerebellar ataxia in moonwalker mice. *Proc Natl Acad Sci USA* 106(16):6706–6711.
86. Myers BR, Bohlen CJ, Julius D (2008) A yeast genetic screen reveals a critical role for the pore helix domain in TRP channel gating. *Neuron* 58(3):362–373.
87. Loukin S, Su Z, Zhou X, Kung C (2010) Forward genetic analysis reveals multiple gating mechanisms of TRPV4. *J Biol Chem* 285(26):19884–19890.
88. Rock MJ, et al. (2008) Gain-of-function mutations in TRPV4 cause autosomal dominant brachyolmia. *Nat Genet* 40(8):999–1003.
89. Di Palma F, et al. (2002) Mutations in Mcoln3 associated with deafness and pigmentation defects in varitint-waddler (Va) mice. *Proc Natl Acad Sci USA* 99(23): 14994–14999.
90. Kim HJ, et al. (2007) Gain-of-function mutation in TRPML3 causes the mouse Varitint-Waddler phenotype. *J Biol Chem* 282(50):36138–36142.
91. Su Z, et al. (2007) Yeast gain-of-function mutations reveal structure-function relationships conserved among different subfamilies of transient receptor potential channels. *Proc Natl Acad Sci USA* 104(49):19607–19612.